

Journal of Biomedical Optics

SPIEDigitalLibrary.org/jbo

Shear flow-induced optical inhomogeneity of blood assessed *in vivo* and *in vitro* by spectral domain optical coherence tomography in the 1.3 μm wavelength range

Peter Cimalla
Julia Walther
Matthaeus Mittasch
Edmund Koch

Shear flow-induced optical inhomogeneity of blood assessed *in vivo* and *in vitro* by spectral domain optical coherence tomography in the 1.3 μm wavelength range

Peter Cimalla,* Julia Walther,* Matthaeus Mittasch, and Edmund Koch

Dresden University of Technology, Clinical Sensing and Monitoring, Faculty of Medicine Carl Gustav Carus, Dresden, 01307 Germany

Abstract. The optical inhomogeneity of flowing blood, which appears as a waisted double fan-shaped intensity pattern inside vessels in cross-sectional optical coherence tomography (OCT) images, was investigated for the first time. High resolution spectral domain OCT in the 1.3 μm wavelength region is used to assess this inhomogeneous intravascular backscattering of light in an *in vivo* mouse model and flow phantom measurements. Based on a predicted alignment of the red blood cells toward laminar shear flow, an angular modulation of the corresponding backscattering cross-section inside the vessels is assumed. In combination with the signal attenuation in depth by absorption and scattering, a simple model of the intravascular intensity modulation is derived. The suitability of the model is successfully demonstrated in the *in vivo* experiments and confirmed by the *in vitro* measurements. The observed effect appears in flowing blood only and shows a strong dependency on the shear rate. In conclusion, the shear-induced red blood cell alignment in conjunction with the vessel geometry is responsible for the observed intensity distribution. This inherent effect of blood imaging has to be considered in attenuation measurements performed with OCT. Furthermore, the analysis of the intravascular intensity pattern might be useful to evaluate flow characteristics. © 2011 Society of Photo-Optical Instrumentation Engineers (SPIE). [DOI: 10.1117/1.3653235]

Keywords: optical coherence tomography; blood flow imaging; shear flow; red blood cell alignment; *in vivo*; flow phantom.

Paper 11222PR received May 6, 2011; revised manuscript received Aug. 25, 2011; accepted for publication Sep. 26, 2011; published online Oct. 31, 2011.

1 Introduction

In optical coherence tomography (OCT), low-coherent near-infrared light backscattered from tissue boundaries is employed to obtain cross-sectional information of tissue microstructure. Due to its high spatial resolution of several micrometers and the ability of real-time imaging, OCT allows noninvasive and contactless investigation of high dynamic microscopic processes like blood flow in small vessels with a diameter less than 500 μm . Figure 1 shows an *in vivo* cross-sectional OCT image of the murine saphenous artery and vein surrounded by perivascular tissue. The appearance of the corresponding tissue in the OCT image is primarily defined by its scattering and absorption properties. In spite of blood being a highly scattering medium in the near-infrared range, an unexpected inhomogeneous intensity distribution inside the blood vessels becomes increasingly visible when several time-resolved cross-sectional images are averaged in order to suppress speckle noise of the flowing media. The lateral zones of the vessel lumen appear as a low-scattering part compared to the superficial and the profound regions resulting in a waisted double fan-shaped intensity pattern which resembles the shape of a sand glass. This effect, which shows similarities to a catacaustic being produced by the envelope of light rays reflected or refracted

by spherical surfaces, is also observable in images of human retinal blood vessels *in vivo* published by others.^{1,2}

As the scattering of blood is mainly caused by its cellular components³ with a majority of red blood cells (RBCs), probably their intravascular orientation is responsible for the observed intensity pattern. Already in 1922, Jeffrey published a theoretical paper about the motion of ellipsoid particles immersed in a viscous liquid.⁴ By his calculations, he found that these particles, which are a good approximation for human erythrocytes, have a preferential orientation toward laminar flow. In 1969, Schmid-Schönbein and Wells have presented that RBCs in highly viscous media show fluid drop-like flow properties.⁵ The initially biconcave RBCs become progressively deformed into prolate ellipsoids with increasing shear flow, their long axis parallel aligned to the flow direction. The cell membrane of the erythrocytes rotates around the intracellular medium (tank-treading) which greatly reduces viscosity at high shear rates. In 1986, Bitbol investigated the orientation of erythrocytes in diluted suspension with a rheoscope and presented three elementary results.⁶ First, for very low shear rates, the RBCs are randomly aligned in the shear flow undergoing a tumbling motion. Second, at intermediate shear stresses $< 1 \text{ N/m}^2$, the erythrocytes spin around their symmetry axis which is aligned to the vorticity axis of the shear field (orbit "C = 0") and consequently the erythrocytes are seen rim-on from the vessel wall. Third, for higher shear stresses, the erythrocytes elongate and align themselves toward the flow in a way that their disk plane is almost parallel to the vessel wall and they are seen face on. Also, the tank-treading motion occurs in

*Each of these authors made essential contributions to the research.

Address all correspondence to: Peter Cimalla, Clinical Sensing and Monitoring, Faculty of Medicine Carl Gustav Carus, Dresden University of Technology, Fetscherstraße 74, Dresden, 01307 Germany; Tel: +49 351 458 6139; Fax: +49 351 458 6325; E-mail: peter.cimalla@tu-dresden.de.

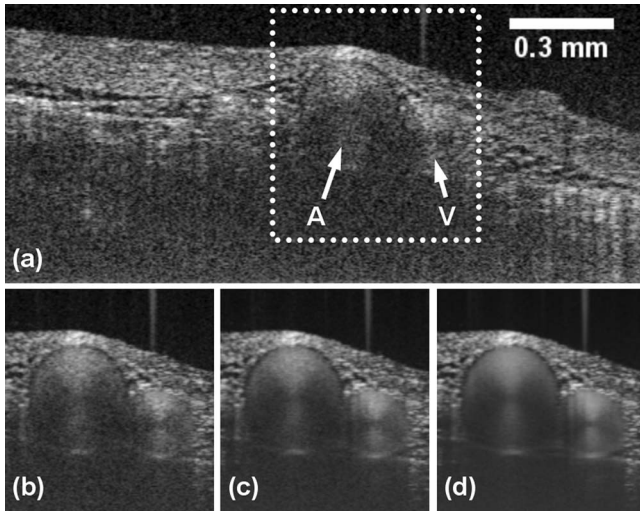


Fig. 1 (a) Cross-sectional OCT image of the saphenous artery (A) and vein (V) of the mouse *in vivo* obtained in the $1.3 \mu\text{m}$ wavelength region. The section denoted by the dotted rectangle was averaged over 5 (b), 21 (c), and 95 (d) time-resolved B-scans in order to suppress speckle noise. In both blood vessels a waisted double fan-shaped intensity pattern becomes clearly visible.

this position. In the recent literature, characteristic changes in morphology and organization of the RBCs are linked to various ranges of shear rate.⁷ At low shear rates $<60 \text{ s}^{-1}$ or no flow, the RBCs form rouleaux-shaped aggregates induced by plasma proteins. Washed RBCs in saline solution form no aggregates and are randomly orientated. At shear rates between 100 and 200 s^{-1} , the aggregates are disintegrated and the RBCs show random orientation in plasma. In the range 200 to 600 s^{-1} , the RBCs start to align to the flow and are finally elongated to ellipsoids at shear rates exceeding 600 to 1000 s^{-1} .

The optical properties of blood in motion have been investigated with a variety of devices and techniques like rheoscopy,^{5,6} light scattering, and absorption measurements in flow cuvettes⁷⁻¹⁰ and laser diffraction (ektacytometry).¹¹ In the present study, for the first time, the flow-dependent behavior of RBCs under *in vivo* and *in vitro* conditions is investigated in a depth-resolved manner using high resolution spectral domain OCT. The flow-induced orientation of the RBCs will lead to an angular modulation of the backscattering cross-section in the blood vessel resulting in a characteristic OCT intensity pattern as shown in Fig. 1. This effect has to be considered in the field of velocity determination by means of OCT sig-

nal power decrease,^{12,13} blood absorption, and scattering measurements with OCT concerning the assessment of hemoglobin oxygen saturation level^{14,15} and flow-induced axial migration of RBCs,¹⁶ as well as in optical coherence angiography.¹⁷ Furthermore, the analysis of the shape of the intravascular OCT intensity pattern might be a useful tool to evaluate flow characteristics.

In the following work, the intravascular backscattering distribution is investigated in an *in vivo* mouse model,¹⁸ as well as in flow phantom measurements and a simple model of the angular intensity modulation in blood vessels based on the RBC orientation toward the flow is described.

2 Methodology

2.1 Theoretical Model

Based on the above-mentioned view of the RBC behavior in shear flow, the following theoretical model of the resulting optical inhomogeneity of flowing blood is derived. At resting conditions or at very low shear rates, the RBCs are randomly orientated or form rouleaux-shaped aggregates. At physiological shear rates induced by the normal blood flow, the RBCs are aligned in a way that their symmetry axis is almost parallel to the gradient of the flow velocity field. In the case of laminar flow in a tube-like blood vessel, the velocity gradient has only a component in radial direction. This means that the RBCs are orientated with their disk plane running almost parallel to the vessel wall. At the same time, the tank-treading motion of the RBC membrane occurs which effectively drains the shear forces at the cell surface and therefore protects the inner RBC components. Toward higher shear rates, the RBCs are additionally elongated to ellipsoids. Figures 2(a)–2(c) summarize the assumptions made about the RBC alignment behavior under shear flow conditions.⁷ Due to their parallel alignment toward the vessel wall, the RBCs are seen rim-on at the lateral zones and face-on at the superficial and profound regions of a tube-like blood vessel, as shown in Fig. 2(d). Concerning the optical properties, the backscattering cross-section of RBCs seen face-on must be relatively high due to the large amount of area that is exposed to the incident light in an approximately perpendicular manner. Compared to that, the backscattering at RBCs seen rim-on must be relatively low. As a consequence, the varying angle of the RBCs to the incident light as a function of their position in the vessel cross-section will lead to a circumferential modulation of the intravascular backscattering which is rotationally symmetric with respect to the vessel center.

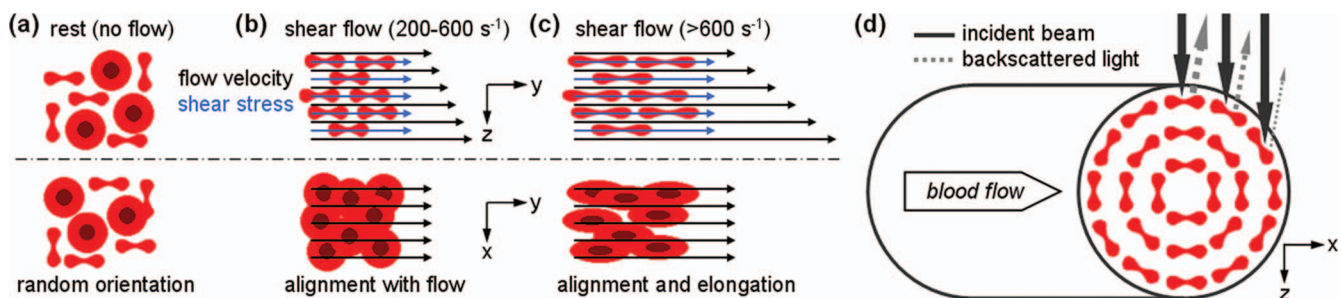


Fig. 2 RBC alignment behavior under shear flow conditions at rest (a), moderate (b), and high shear flow (c). In tube-like blood vessels, the RBCs are orientated with their disc plane running almost parallel to the vessel wall under laminar flow conditions (d) which will lead to a circumferential modulation of the intravascular backscattering cross-section. (Color online only.)

Let z be the axial scan direction of the OCT beam, y the direction of the transverse flow component, and x the lateral scan direction of the OCT beam, which is perpendicular to y . If the orientation of the disk-shaped RBCs toward the flow and a corresponding circumferential modulation of the backscattering cross-section is responsible for the observed double fan-shaped intensity pattern inside the blood vessels, a harmonic modulation of the image intensity along a circular path S centered at the midpoint $M(x_0; z_0)$ of the vessel will occur. With the distance r between S and M the circular path S can be described in Cartesian coordinates by Eq. (1),

$$S(x - x_0; z - z_0) = S(-r \cdot \sin \varphi; -r \cdot \cos \varphi). \quad (1)$$

In this situation, φ is the angle of rotation of S with respect to the z -axis which corresponds to the direction of the incident light. The harmonic modulation of the pixel intensity I , which represents the logarithmic OCT signal power, can then be described along the circular path S by Eq. (2),

$$I(z; \varphi) = I_0 + I_1(z) + \hat{I}_2 \cdot \cos(2\varphi). \quad (2)$$

The term $\hat{I}_2 \cdot \cos(2\varphi)$ is used as the simplest factor with respect to the symmetry of the red blood cells and I_0 as the general signal background. The term $I_1(z)$ represents the depth-dependent signal component caused by sample absorption and scattering. In the single scattering region, light propagating through a homogeneous absorbing or scattering medium is exponentially attenuated in depth according to Beer–Lambert’s law.¹⁹ If we assume that this effect is the dominant attenuation mechanism, then the pixel intensity as the logarithmic OCT signal power shows an approximately linear decrease in depth. Hence, $I_1(z)$ with respect to the rotation angle φ can be expressed in first order by another cosine term given by Eq. (3),

$$I_1(z) = \hat{I}_1 \cdot \cos(\varphi). \quad (3)$$

The harmonic intensity modulation along the circular path S in dependency of φ can then be written as Eq. (4).

$$I(\varphi) = I_0 + \hat{I}_1 \cdot \cos(\varphi) + \hat{I}_2 \cdot \cos(2\varphi). \quad (4)$$

The right side of Eq. (4) represents the first terms of a Fourier series. So, in general, one can perform a discrete Fourier analysis of the pixel intensity data. Depending on the number of data points on the circle, the series contains all frequencies from zero to the Nyquist frequency. Selecting $2n$ data points on the circle, the general form of the series is given by Eq. (5),

$$I(\varphi) = \sum_{k=0}^n \hat{I}_k \cdot \cos(k \cdot \varphi) + \sum_{k=1}^{n-1} B_k \cdot \sin(k \cdot \varphi). \quad (5)$$

While the \hat{I} -coefficients still represent the symmetric pixel intensity, the B -coefficients describe an asymmetry between the left and right side of the circle that is only found in rare cases, e.g., when a shadow masks a part of the vessel. Data with structures causing a strong shadow within the vessel lumen have not been analyzed. Consequently, the B -coefficients in general are small and will not be presented. The high order coefficients are influenced by the noise (e.g., speckle) in the data while the low order coefficients yield the information about damping and scattering asymmetry. In general, it was found empirically that the coefficients drop very fast to a constant noise level and only the first four coefficients have a sufficient impact. As a consequence, the

intensity modulation along the circular path S is more precisely described by Eq. (6),

$$I(\varphi) = I_0 + \hat{I}_1 \cdot \cos(\varphi) + \hat{I}_2 \cdot \cos(2\varphi) + \hat{I}_3 \cdot \cos(3\varphi) + \hat{I}_4 \cdot \cos(4\varphi). \quad (6)$$

In summary, the zeroth-order and first-order coefficients represent the general intensity background and the linear damping of the logarithmic OCT signal in depth, respectively. The second- and fourth-order coefficients describe the angular change of the RBC backscattering cross-section with respect to their symmetry. The third-order coefficient stands for a nonlinear drop of the OCT signal in depth which could be caused by multiple scattering or the focusing of the scanning OCT beam.

2.2 Experimental Setup

A spectral domain OCT system operating in the 1.3- μm wavelength region is applied which enables an enhanced penetration depth into blood vessels due to the low absorption of hemoglobin and the reduced scattering of blood in this spectral range. The setup is part of a simultaneous dual-band OCT system presented recently²⁰ with a full spectral width of 300 nm centered at 1250 nm. The system is illuminated by a commercially available supercontinuum laser light source (SuperK Versa, Koheras A/S, Denmark) and allows three-dimensional (3D) imaging with a high axial resolution better than 7 μm in air over the entire depth measurement range and an A-scan rate of up to 47 kHz. The lateral resolution in air was measured to be 9.7 μm and the sensitivity amounts to -91 and -87 dB at an A-scan rate of 12 and 36 kHz, respectively. The control of the system, the data acquisition, and the processing is done by means of a personal computer and custom software developed with LABVIEW (National Instruments, USA).

2.3 Extraction of Flow Velocity and Shear Rate from OCT Data

In order to investigate the dependency of the optical inhomogeneity of blood on the flow velocity and the shear rate, both parameters are extracted from the OCT data via phase-resolved Doppler analysis.^{21,22} Using the classic Doppler model, the flow velocity at a certain axial depth z can be determined by Eq. (7),

$$v(z) = \frac{\Delta\varepsilon(z) \cdot \lambda_0}{4\pi \cdot T \cdot n_{\text{medium}} \cdot \sin \vartheta}, \quad (7)$$

where $\Delta\varepsilon$ is the phase difference between adjacent A-scans due to the Doppler shift, λ_0 is the center wavelength, T is the time period between adjacent A-scans, n_{medium} is the refractive index of the flow medium, and ϑ is the Doppler angle between the light beam in the flow medium and the perpendicular of the velocity vector. The classic Doppler model can be used instead of the new Doppler model found by our group²² since no or only little phase wrapping occurred during the measurements and deviations between classic and new Doppler model are found to be small within the first phase wrapping period for Doppler angles larger than 5 deg in the 1.3 μm wavelength range. However, the Doppler angle is affected by light refraction on sample surfaces above the blood vessel. For small angles, it can be determined via Eq. (8) using the optical inclination angle δ of the blood

vessel, which can be easily extracted from previously recorded three-dimensional OCT image data.

$$\vartheta = \frac{\delta}{n_{\text{medium}}}. \quad (8)$$

For round shaped blood vessels, this can be applied only in the vessel center, where lateral light refraction due to spherical vessel surfaces can be neglected. Hence, using Eqs. (7) and (8), the flow velocity can be determined for small angles without knowledge of the refractive indices of neither the flow medium, i.e., blood, nor the tissue covering the blood vessel. A special case is a glass capillary immersed in air as often used for flow phantom measurements. Assuming parallelism of the capillary walls, the correct Doppler angle can be calculated also for large angles via Eq. (9),

$$\sin \vartheta = \frac{n_{\text{air}}}{n_{\text{medium}}} \cdot \sin \delta, \quad (9)$$

where $n_{\text{air}} \approx 1$ is the refractive index of air. Hence, in this situation, the flow velocity can be determined very precisely using Eqs. (7) and (9) without knowledge of the refractive indices of the glass capillary or the flow medium.

The shear rate is the spatial derivative of the flow velocity. Assuming laminar flow, the parabolic flow velocity profile v along the vessel radius r can be expressed by Eq. (10),

$$v(r) = v_{\text{max}} \left[1 - \left(\frac{r}{R} \right)^2 \right], \quad (10)$$

where v_{max} is the maximum flow velocity in the vessel center at $r = 0$ and R is the total vessel radius. Hence, the corresponding shear rate distribution γ can be determined by Eq. (11),

$$\gamma(r) = \left| \frac{dv(r)}{dr} \right| = \frac{2v_{\text{max}}}{R^2} \cdot r. \quad (11)$$

Therefore, the shear rate at a certain radius can be easily extracted by measuring the total vessel radius and the maximum flow velocity by OCT and Doppler OCT, respectively.

3 In Vivo Measurements

In order to investigate the intravascular backscattering distribution under *in vivo* conditions, a mouse model was applied in which the saphenous blood vessels located at the hind limb were transilluminedly imaged by OCT.¹⁸ All experiments were performed in accordance with the *Guide for the Care and Use of Laboratory Animals* (Institute of Laboratory Animal Resources, 7th Ed., National Academy Press, Washington, D.C., 1996). The study was approved by the governmental animal care and use committee. Cross-sectional OCT scans of the murine saphenous artery and vein were recorded over several heart cycles at an A-scan rate of 36 kHz and an exposure time of 23.8 μ s. The image size was 576 A-scans per B-scan, which resulted in a frame rate of 62.5 fps. The recorded time-resolved B-scan stack consisted of 448 images, which corresponds to a time period of 7.168 s. In order to suppress any effects of the pulsatile flow in the artery, only cross-sectional scans at defined states of the heart cycle were analyzed, i.e., the systolic and diastolic point of time corresponding to the highest and lowest occurring arterial flow velocity and the equilibrium where temporary no flow is present in the artery. These states, shown in Fig. 3, were found

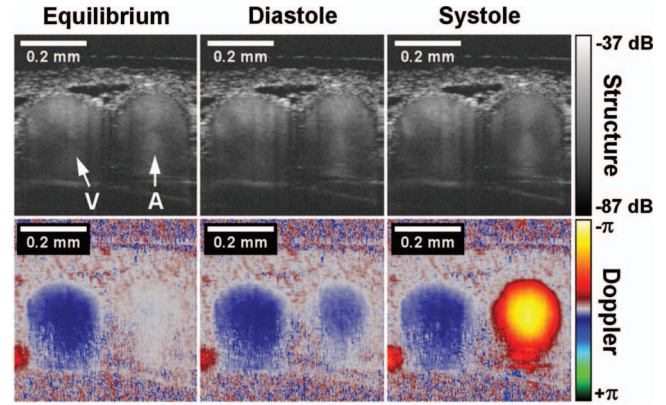


Fig. 3 Structural OCT images and corresponding color-encoded Doppler phase shift distributions of the murine saphenous artery (A) and vein (V) *in vivo* during three states of the heart cycle: equilibrium (temporary no flow present in the artery), diastole (slightly retrograde flow in the artery) and systole (maximum flow in the artery). The images were obtained by averaging the corresponding cross-sectional scans of 16 consecutive heart cycles. In all three heart cycle states, a double fan-shaped intensity distribution can be identified in the artery as well as in outlines in the vein. (Color online only.)

by means of phase-resolved Doppler analysis of the raw image data as described in Sec. 2.3. In order to suppress speckle noise in the highly scattering blood, the corresponding cross-sectional scans of 16 consecutive heart cycles were averaged. In the artery, a double fan-shaped intensity distribution can be identified during the systole and equilibrium as well as during the diastole, where a slightly retrograde flow is present. Also in the vein, a slight double fan-shaped intensity distribution is visible.

The pixel intensity as the logarithmic reflectance of the sample with respect to an ideal mirror was then recorded along a circular path centered at the midpoint of the artery as shown in Fig. 4(a). The radius of this circular path is half of the entire vessel radius. To validate the assumption of the linear signal

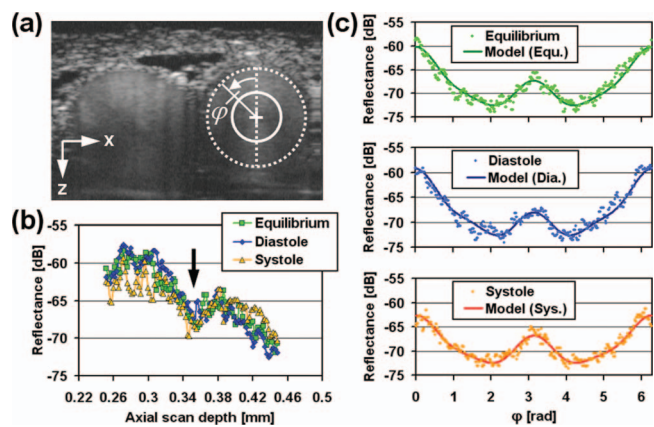


Fig. 4 (a) Murine saphenous blood vessels with marked arterial vessel wall (dashed circle), vertical symmetry line (dashed line) and half vessel diameter circular path (solid circle) centered at the artery midpoint (cross). (b) Signal attenuation across the murine saphenous artery recorded along the dashed line in (a) for the three heart cycle states. In all states, the attenuation is approximately linear in depth as predicted in the model. The intensity dip in the vessel center (arrow) is probably caused by RBC tumbling. (c) Signal modulation along the green circular path in (a) and fitted model described by Eq. (6) for the three heart cycle states. (Color online only.)

attenuation in depth by means of absorption and scattering, the intensity across the artery along the vertical symmetry line was also analyzed. In Fig. 4(b), it can be seen that the signal attenuation is approximately linear in depth in all three heart cycle states as predicted in the theoretical model. In the center of the blood vessel, an intensity dip can be observed. This is probably caused by RBC tumbling or random orientation due to the low shear forces that are present at this location. Under laminar flow conditions, the local shear rate as the gradient of the flow velocity field equals zero at the vessel center and increases in radial direction toward the vessel wall. As a consequence, the RBCs at the vessel center are not aligned compared to the face-on aligned RBCs on the vertical symmetry line above and below. This leads to the observed local decay of the backscattering cross-section at the vessel center. Figure 4(c) shows the recorded intensity along the circular path plotted in combination with the quadruple cosine model described by Eq. (6). The model was fitted to the data using the intensity amplitudes \hat{I}_0 to \hat{I}_4 as free parameters. It can be seen that the model is in good agreement with the data and a circular intensity modulation can be observed in all three investigated states of the heart cycle. The occurrence of the circular intensity modulation in the diastole and the systole is coincident with the predicted intravascular alignment of the RBCs due to the presence of shear flow. The fan-shaped intensity pattern during the equilibrium, where temporarily no flow is present, can be explained by the time response of the RBC orientation. The disorientation process of the RBCs at no flow takes longer than the time until the next heart beat occurs. Therefore, the circular intensity modulation is maintained over the entire heart cycle.

Figure 5 summarizes the flow characteristics within the saphenous blood vessels of the investigated mouse, which were again analyzed by means of the phase-resolved Doppler method. The optical inclination of the blood vessels was measured to be 14.4° using previously recorded 3D OCT data. Hence, the Doppler angle was estimated to be 10.4 deg via Eq. (8) using $n = 1.39$ as refractive index for blood. It can be seen that the Doppler flow signal across the blood vessels can be described by parabolic functions which leads to the conclusion that laminar flow is present in the artery as well as in the vein. Thereby, the artery shows a pulsatile and bidirectional laminar flow with peak velocities at the vessel center of approximately 40 and -4 mm/s during the systole and diastole, respectively. As expected, an approximately stationary flow is present in the vein with a flow velocity of approximately -5 mm/s at the vessel center. The heart rate was measured to be 139 beats per minute which corresponds to a heart cycle duration of 0.432 s. This low heart rate was due to deep anesthesia applied in the mouse model, as described elsewhere.¹⁸ In conclusion, the results show that the theoretically predicted intravascular orientation of the RBCs under laminar flow conditions could be the reason for the observed inhomogeneous backscattering distribution inside the blood vessels.

4 In Vitro Measurements

4.1 Flow Phantom Model

In order to investigate the stationary and dynamic properties of the circular intensity modulation in conjunction with the orientation of the RBCs toward the shear flow, a flow phantom with

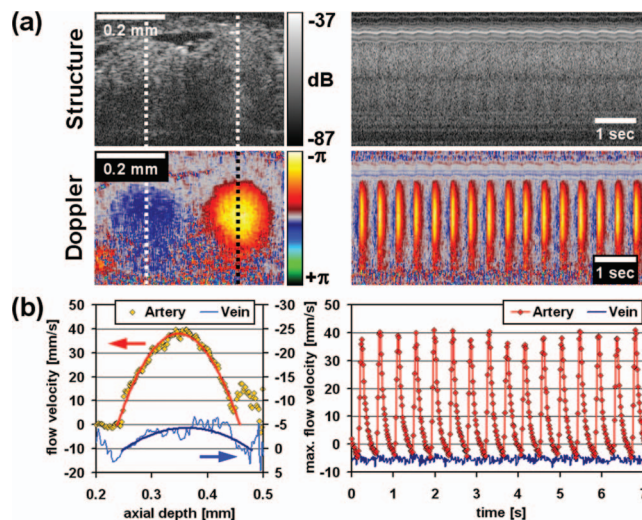


Fig. 5 (a) Single structural OCT image and color-encoded Doppler phase shift distribution showing the murine saphenous artery and vein *in vivo* during the systole (left) and corresponding pseudo M-scans across the center of in the artery obtained by reslicing the recorded B-scan stack (right). (b) Extracted flow velocity profiles from the Doppler signal across the blood vessels (left) and maximum flow velocities plotted over time (right). The positions of the respective flow profiles are indicated by the dashed lines in (a). The laminar arterial and venous blood flow are represented by the red and blue parabola, respectively, fitted to the Doppler signal. The maximum flow velocity on the right was obtained from the vertex of the parabolic fit. A pulsatile bidirectional flow in the artery and an approximately stationary flow in the vein are present. (Color online only.)

well-known flow characteristics was applied. A flow-controlled infusion pump (Injectomat MC Agilia D, Fresenius Vial, France) was used to create a stationary laminar flow in two different glass capillaries with circular and square cross-section and a nominal inner diameter of 0.2 mm. Human whole blood, taken from a young healthy volunteer, and 1% Intralipid emulsion were used as flow media. It is noteworthy that the size of human RBCs is comparable to those of mice.²³ Consequently, similar results compared to the *in vivo* experiments are expected for the flow phantom measurements. The inclination angle δ of the square and circular capillary was extracted from 3D OCT data and amounted to 7.1 and 7.0 deg, respectively. The refractive index of the flow media was measured to be 1.34 for 1% Intralipid emulsion and 1.39 for human whole blood. Hence, the Doppler angle ϑ was in the range of 5 deg. With Eqs. (7) and (9), the resulting unique flow velocity measurement range at an A-scan rate of 36 kHz was calculated to be ± 92 mm/s before phase wrapping occurs. Single phase wrapping at higher flow velocities was corrected by a simple unwrap algorithm. A phase shift of 2π was added to negative Doppler phase shifts at positive flow and subtracted from positive Doppler phase shifts at negative flow. The correct flow direction (positive or negative) was known *a priori* due to measurements at low flow velocities without phase wrapping.

4.2 Stationary Behavior

In a first step, the development of the double fan-shaped intensity pattern was investigated in dependency of an applied constant stationary flow in the square and circular capillaries.

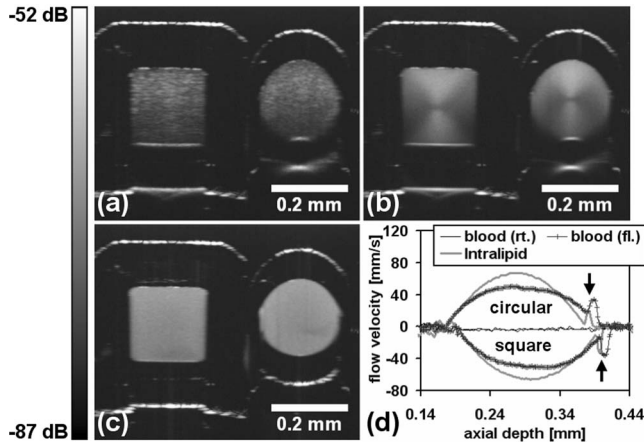


Fig. 6 Cross-sectional OCT images of a circular and square glass capillary perfused in opposite directions with human whole blood at (a) resting (rt.) and (b) flowing (fl.) conditions, as well as (c) flowing 1% Intralipid emulsion. The parabolic flow velocity profiles yielded at the vertical vessel symmetry lines by means of phase-resolved Doppler analysis (d) indicate that laminar flow is present in the capillaries. The arrows denote Doppler shadows at posterior lumen walls. Posterior displacement of Intralipid and blood Doppler signals indicates different refractive index of flow media.

Although the above measured highest flow velocities *in vivo* amount to approximately 40 mm/s, it was shown that the maximum flow velocity in the saphenous artery of an anesthetized mouse can be up to 70 mm/s during the systole.²⁴ Therefore, the flow delivered by the infusion pump is adjusted in a way that comparable flow velocities and resulting shear rates are present in the glass capillaries. Since the small glass capillaries form a large flow resistance, it cannot be guaranteed that the given flow value is fully delivered by the infusion pump. Therefore, the given flow serves as a coarse value only. The exact flow velocity is subsequently measured by means of phase-resolved Doppler OCT as described in Sec. 2.3. Under the assumption that laminar flow is present, the mean flow velocity in the circular and square capillary can be calculated by multiplying the maximum flow velocity value in the vessel center by a factor of 0.5 and 0.477, respectively.

Figure 6 shows cross-sectional OCT images of the circular and square glass capillary immersed in air, which were perfused in opposite directions with 1% Intralipid emulsion as well as human whole blood under flowing and resting conditions. These images were found by averaging 256 B-scans recorded at an A-scan rate of 36 kHz in order to suppress speckle noise. The flow delivered by the infusion pump was adjusted in a way that a similar maximum flow velocity as in the murine saphenous artery during the systole is present in the blood and Intralipid perfused capillaries. Due to light refraction at the spherical surfaces of the circular capillary, the capillary's lumen appears laterally expanded in the OCT image. This optical distortion was corrected in first order by lateral image scaling with an empirically found factor of 0.76. Ray tracing simulations (OSLO Light Edition 6.4, Lambda Research,) revealed that remaining lateral and axial image distortion of the circular capillary lumen is negligible for our analysis. It can be seen that the effect of an inhomogeneous backscattering intensity pattern is present only at flowing blood in both the circular as well as the square capil-

lary. The effect is absent at resting blood and flowing Intralipid emulsion. These results confirm the assumption that the shear flow-induced alignment of the RBCs is responsible for the observed effect. Because the effect is also distinctively developed in the square capillary, it cannot be caused by some catacaustic phenomena produced by the spherical optical surfaces of the circular capillary. In order to verify that laminar flow is present, the parabolic flow velocity profiles were also evaluated by means of phase-resolved Doppler analysis.

The backscattering intensity distribution of flowing blood shown in Fig. 6(b) is investigated more closely in Fig. 7. In a first step, the intensity profiles across the vertical and horizontal symmetry lines for both the square and circular capillary are plotted in Figs. 7(a) and 7(b), respectively. In both capillary centers, an intensity dip in the vertical (axial) profile and an intensity peak in the horizontal (lateral) profile can be observed. This is probably caused by the RBC tumbling motion due to the low shear forces at this location. In a vertical direction, the RBCs are assumed to be aligned face-on, which results in an intense backscattering signal. In the center, the RBCs are randomly aligned due to the tumbling motion. Therefore, the mean backscattering intensity must be lower at this location compared to the superficial and profound regions of the lumen which is represented by the intensity dip. In contradiction, the RBCs at the horizontal symmetry line are seen rim-on resulting in a lower backscattering signal. In comparison, the mean backscattering intensity from the randomly orientated RBCs in the center must be higher which is represented by the intensity peak. Averaging of the $\cos(2\varphi)$ term over all RBC orientations in three dimensions results in a mean value of $-1/3$ which explains why the peak in the horizontal direction is only approximately half the magnitude of the dip in the vertical direction. These observations are consistent with the *in vivo* measurements described in Sec. 3. Comparing the profiles of backscattering, an increased intensity at the lateral edges of the circular capillary can be observed. These lateral intensity side lobes are caused by less signal attenuation in depth due to shorter optical propagation path lengths through blood in the lateral zones compared to the center zone of a circular lumen. In the square capillary, these propagation path lengths are ideally identical, i.e., there are no lateral intensity side lobes. Figures 7(c) and 7(d) show the recorded intensity along three different circular paths centered at the capillary midpoints. The circular paths are defined by a relative radius which is the quotient of the geometrical measurement radius r and the entire capillary radius R . The data is plotted in combination with the fitted quadruple cosine model described by Eq. (6). It can be seen that a circular intensity modulation, which is comparable to the *in vivo* measurements, is also present under *in vitro* conditions, and that the fitted model again is in good agreement with the obtained data, for both square and circular capillary. Furthermore, the circular intensity modulation is mainly characterized by the first-order (one oscillation per period) and second-order (two oscillations per period) coefficients which represent the linear intensity attenuation in depth and the angular change of the RBC backscattering cross-section with respect to their symmetry, respectively. The positive fourth-order coefficient shows that RBC reflection is more specular than described by a pure second-order coefficient. In order to find a measure for the development of the inhomogeneous intensity pattern, both coefficients are plotted over the relative measurement radius for the square and circular

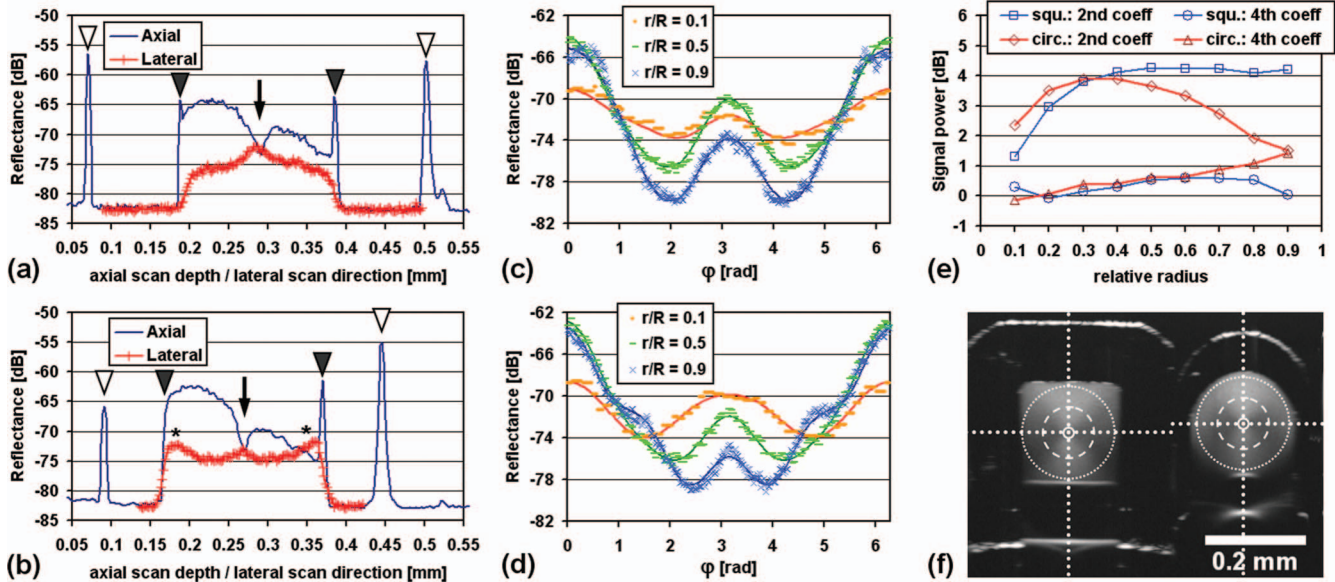


Fig. 7 Investigation on the backscattering intensity distribution of flowing human whole blood. (a) and (b) Intensity profiles across the vertical (blue) and horizontal (red) vessel symmetry line [dotted white lines in (f)] for the square (a) and circular capillary (b). The bright and dark arrowheads denote the outer and inner capillary diameter, respectively. An intensity dip in the axial profile and an intensity peak in the lateral profile (arrows) can be observed in the vessel center. The asterisks indicate lateral intensity side lobes in the circular capillary. (c) and (d) Circular intensity modulation along three different paths with 10%, 50%, and 90% of the entire vessel diameter (solid, dashed, and dotted circles in (f), respectively) and corresponding fitted model (solid lines) for the square (c) and circular capillary (d). (e) Second- and fourth-order coefficients of the fitted model plotted over the relative measurement radius for the square (blue) and circular capillary (red). (f) Corresponding OCT image of the circular and square glass capillary perfused with human whole blood. (Color online only.)

capillary in Fig. 7(e). It can be seen that the dominant second-order coefficient increases with the relative radius, reaches its maximum at approximately 40% to 50%, and remains constant toward larger relative radii in the square capillary. In the circular capillary, the second-order coefficient declines again while the fourth-order coefficient significantly increases. This is not a true effect of the RBC alignment but an artifact caused by the lateral intensity side lobes in the circular capillary. Hence, for further measurements, the circular intensity modulation is evaluated at 50% of the entire lumen radius, as proposed in the *in vivo* measurements section, and the second-order coefficient of the fitted model is used for quantification in order to guarantee maximum sensitivity to the development of the double fan-shaped intensity pattern.

4.3 Flow-Dependent Behavior

In a next step, the dependency of the intravascular backscattering distribution on the flow velocity is investigated. Due to the fact that square blood vessels do not appear in the physiological *in vivo* situation, this measurement was performed in the circular capillary only. Fig. 8(a) shows cross-sectional OCT images of a circular glass capillary perfused with human whole blood at different mean flow velocities which were estimated using phase-resolved Doppler analysis. These images again were generated by averaging 256 B-scans recorded at an A-scan rate of 36 kHz in order to suppress speckle noise. In all images, the double fan-shaped intensity pattern can be identified apart from the images recorded at 0 mm/s. In this situation, despite averaging, the blood shows a speckle pattern due to the complete

absence of flow. All images were analyzed according to Sec. 3 and as described above. Figure 8(b) shows the obtained circular intensity modulation evaluated at 50% of the entire capillary radius plotted in combination with the fitted model described by Eq. (6). Again, the data and the predicted model show good correspondence to each other. In order to assure that the local minima of the intensity modulation are not clipped by the limited sensitivity of the OCT system, also the noise floor of the images is evaluated. It can be seen that all intravascular intensity values of interest are well above the noise level. The second-order coefficient of the fitted model as a direct measure for the development of the double fan-shaped intensity pattern is plotted over the applied mean flow velocity in Fig. 8(c). The corresponding shear rate at 50% of the capillary radius was calculated predicting a radial symmetric parabolic flow velocity profile. It can be seen that the development of the double fan-shaped intensity pattern shows a flow-dependent course. At first, it increases with heightening flow velocities, as expected, due to the alignment of the RBCs toward the shear flow. At a shear rate of approximately 300 s^{-1} , the effect reaches its maximum before it starts to decrease again toward higher mean flow velocities above 12 mm/s. A first assumption that this decline process is probably caused by the velocity-dependent signal decrease due to fringe washout^{12,13,25} does not hold true. As the intensity is evaluated on a circular path centered at the capillary midpoint, the corresponding local flow velocity and the resulting signal decrease is supposed to be identical at each position. Consequently, a constant offset is subtracted from the circular intensity values which will have no effect on the modulation itself as long as it is not restricted by the limited sensitivity of the

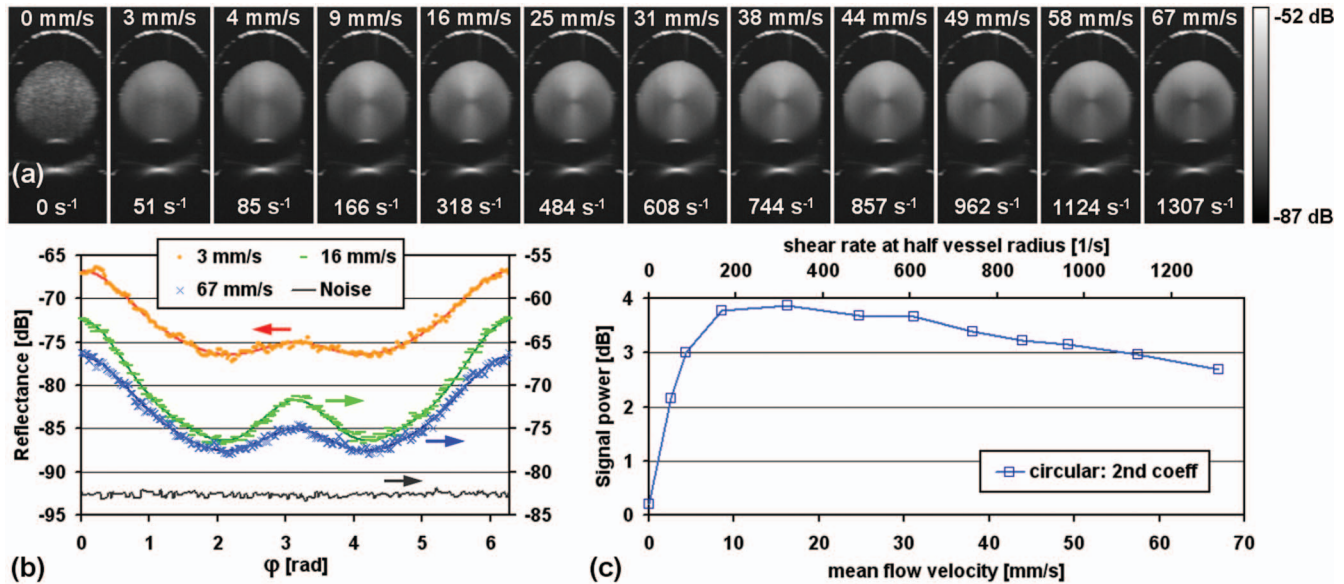


Fig. 8 (a) OCT cross-sectional images of circular glass capillary perfused with human whole blood at different mean flow velocities and resulting shear rates at half vessel radius. The inner diameter of the capillary was measured to be 0.205 mm. (b) Circular intensity modulation at half vessel radius, corresponding fitted model (solid lines) shown exemplarily for three different mean flow velocities and noise floor outside of the capillary at identical axial depth. (c) Second-order coefficient of the fitted model plotted over the mean flow velocity and the corresponding shear rate. (Color online only.)

OCT system. That this is not the case has already been shown in Fig. 8(b) where all circular intensity values of interest are well above the noise level even for the highest applied mean flow velocity of 48 mm/s. As a consequence, further investigations are necessary to elucidate the decline of the double fan-shaped intensity pattern toward higher flow velocities. For this reason, the velocity-dependent intensity profiles along the vertical and horizontal symmetry line of the circular capillary are analyzed in Fig. 9. At low mean flow velocities from 0 to 25 mm/s, a balanced increase of the vertical intensity and the development of the central intensity dip can be observed. This is coincident with the predicted model since the RBCs increasingly align face-on to the incident light but remain randomly orientated in the lumen center. In the horizontal intensity profile, no significant change despite the development of a small central intensity peak

can be identified. At higher mean flow velocities from 31 to 67 mm/s, a radial position-dependent signal decrease due to fringe washout can be observed. The highest signal decrease can be found at the center of capillary where the maximum flow velocity occurs. The horizontal profile shows less signal decrease in the upper and lower third compared to the vertical profile, as indicated by the arrows in Fig. 9(b). A possible explanation for this observation is that the flow-dependent signal decrease induced by fringe washout is superimposed by an additional signal decay caused by RBC elongation toward higher shear rates. If a single RBC is elongated, there will be a decrease in its backscattering cross-section because the amount of surface area that is seen by the OCT sample beam is reduced. As indicated in Sec. 2.2, the sample beam diameter (FWHM) was measured to be $9.7 \mu\text{m}$ in air. For OCT imaging with low

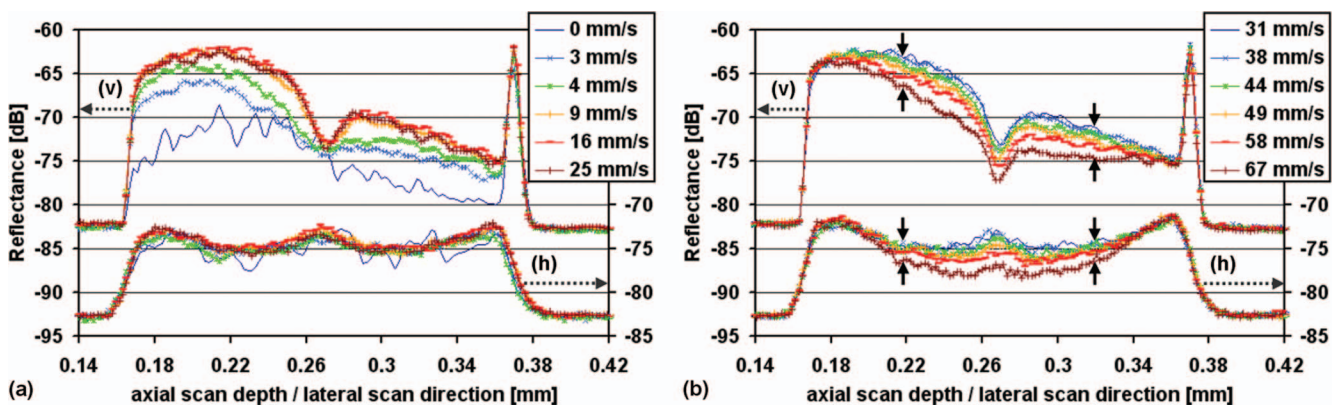


Fig. 9 Intensity profiles across the vertical (v) and horizontal (h) vessel symmetry line of the circular capillary as shown in Fig. 8 for low (a) and high (b) mean flow velocities. The velocity-dependent signal decrease is more pronounced in the vertical direction compared to the horizontal direction (black arrows). (Color online only.)

numerical aperture (0.05), where aberrations due to spherical capillary surfaces can be neglected, the beam diameter should be identical in blood. Hence, it is within the order of magnitude of the diameter of a nonelongated RBC, which amounts to 7 to 8 μm .²³ Therefore, the backscattering reduction will be more severe at a face-on aligned RBC because the elongation-induced change in the surface area seen by the sample beam will be relatively large compared to a rim-on aligned RBC. As a consequence, there is an enhanced signal decrease at the superficial and profound regions compared to the lateral zones of the capillary which is responsible for the decline of the double fan-shaped intensity pattern toward higher flow velocities as observed in Fig. 8(c).

4.4 Dynamic Behavior

In a final step, the dynamic behavior of the double fan-shaped intensity pattern was analyzed. Therefore, a constant flow with a mean flow velocity of 19 mm/s was applied to the circular glass capillary. A time-resolved B-scan stack with 25 frames per second at an A-scan rate of 12 kHz was then recorded over a time period of approximately 40 s. The lower imaging speed was chosen in order to record a longer period of time with respect to the limited size of the data acquisition memory buffer. Approximately 5 s after the start of the recording, the flow in the capillary was halted by simply pinching off the silicon tube between the infusion pump and the glass capillary using a blood vessel clamp. Again, the development of the double fan-shaped intensity pattern was analyzed as described above with the exception that a moving average of only five B-scans was applied to the image stack before analyzing the signal modulation along the circular path and subsequent fitting of the theoretical model. The filter size of five was chosen in order to find a convenient tradeoff between speckle noise suppression and temporal resolution. To compare the structural information with the change of flow inside the capillary, the maximum flow velocity in the capillary center was also evaluated using phase-resolved Doppler OCT. Figure 10 shows the obtained results. It can be seen that the decrease of the second-order coefficient is much slower than the decrease of the flow velocity after pinching off the silicon tube. In order to describe these declines, an exponential function was fitted to the data points given by Eq. (12),

$$A(t) = \hat{A} \cdot e^{-\frac{t-t_0}{\tau}} + A_{\text{Offset}}. \quad (12)$$

In this context, τ is the time constant and t_0 is the point of time when the clamping occurred. After time τ has passed, only 37% of the initial effect is still present. The time constants of the decline of the second-order coefficient and the maximum flow velocity amount to 4.02 and 0.35 s, respectively. This means that the regression of the double fan-shaped intensity pattern takes almost 12 times longer than the time until the flow has come to a complete halt.

5 Discussion

The results of the *in vitro* measurements confirm the observations made in the *in vivo* experiments. There are several facts that indicate that the shear flow-induced orientation of the RBCs is responsible for the observed characteristic waisted double fan-

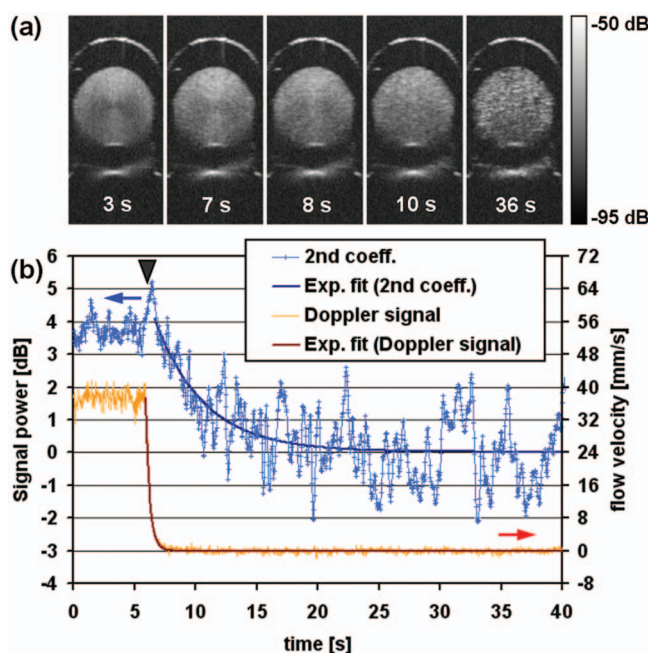


Fig. 10 Dynamic behavior of the inhomogeneous backscattering of flowing blood. (a) OCT cross-sectional images of glass capillary perfused with human whole blood at five different time stages. The flow was stopped approximately 6 s after the start of the recording. The images were found by averaging five subsequent B-scans of the recorded B-scan stack. (b) Second-order coefficient and flow velocity in the capillary center plotted over the recording time of the B-scan stack. The dark arrowhead denotes the point of time when the flow was stopped. The decline of the double fan-shaped intensity pattern is much slower than the decrease of the flow. The time constants of the fitted exponential functions given by Eq. (12) are 4.02 s for the second-order coefficient and 0.35 s for the flow velocity. The increased noise of the second-order coefficient after flow stop is caused by the pronounced speckle as shown in (a) 36 s after the start of the recording. (Color online only.)

shaped intensity distribution inside blood perfused vessels. First of all, the effect is only present in flowing blood as shown in Fig. 6. It is not present at steady state resting blood or flowing 1% Intralipid emulsion. Because these facts apply to both round- and rectangular-shaped capillaries, the effect cannot be caused by some optical catacaustic.

Second, the effect shows a strong dependency on the flow velocity and, as a consequence, on the shear rate as demonstrated in Fig. 8. At first, the effect increases toward higher shear rates which can be explained by a corresponding enhanced alignment of the RBCs. The maximum of the effect, i.e., full alignment of the RBCs, appears approximately between 200 and 300 s^{-1} , which corresponds well to recent literature.⁷ The decline of the effect at higher shear rates above 300 s^{-1} is believed to be caused by an additional shear-induced elongation of the RBCs. Both results, the rise and drop of the effect with increasing shear rate, are confirmed by the anisotropic backscattering behavior of blood along the vertical and horizontal capillary symmetry line as shown in Fig. 9.

A third point is the relatively slow regression of the effect after a sudden elimination of flow as shown in Fig. 10 which can be explained by a slow transition process of the RBCs to the random orientation state in the now shear stress free environment.

While Brownian motion contributes to the random orientation, the main process that drives this transition is believed to be gravitational sedimentation which amounts to 1 to 2 RBC diameters over the observed time constant in physiological blood. This slow regression would also explain why the effect is visible over the entire heart cycle in the *in vivo* measurements even during the equilibrium state where temporarily no flow is present (Figs. 3 and 4). The disorientation of the RBCs just takes much longer than the duration of the heart cycle of the investigated mouse.

Although the applied model of the circular intensity modulation described by Eq. (6) is very simple since a cosine series is used to describe the angular backscattering of RBCs and the signal attenuation in depth, it is suitable to illustrate the fundamental relationship between the predicted alignment of the RBCs toward the shear flow, an angular modulation of the corresponding backscattering cross-section inside the vessel and the resulting OCT signal.

6 Conclusion

The inhomogeneous backscattering distribution of low-coherent light in blood vessels, which appears as waisted double fan-shaped intensity pattern, was investigated in an *in vivo* mouse model and flow phantom measurements using spectral domain OCT in the 1.3 μm wavelength region for high resolution cross-sectional imaging. Based on a predicted alignment of the RBCs toward the laminar shear flow and the signal attenuation in depth by means of absorption and scattering, a simple model of the intravascular intensity modulation along a circular path centered at the vessel midpoint was derived. In a first step, the suitability of the model could be demonstrated by analyzing measurements of the murine saphenous artery imaged at an A-scan rate of 36 kHz. The obtained data and the predicted model show a good correspondence. In a second step, the observed characteristic double fan-shaped intensity pattern could be recreated *in vitro* in a round-shaped as well as a rectangular-shaped glass capillary perfused with human whole blood and the stationary and dynamic properties of the effect were analyzed. The effect appears in flowing blood only and shows a strong flow velocity-dependent behavior attended by an anisotropic change in backscattered intensity which has to be considered in blood attenuation measurements. The results obtained from the *in vitro* measurements confirm the observations made in the *in vivo* experiments leading to the conclusion that the shear-induced alignment of the bi-concave disk shaped RBCs in laminar flow is the reason for the observed inhomogeneous intravascular backscattering distribution. Therefore, the analysis of the intensity pattern inside blood vessels might be a useful tool for the evaluation of flow characteristics regarding laminarity and turbulence or the diagnosis of pathologically shaped RBCs caused by sickle cell anemia or spherocytosis. Furthermore, the flow-dependency of the effect might facilitate an alternative method to measure the flow velocity and shear rate. For future research, more precise computational models of the angular backscattering of the complex-shaped RBCs are considered for final evaluation of the effect, concerning especially the consequences of RBC elongation toward higher shear rates.

Acknowledgments

This research was supported by SAB (Sächsische Aufbaubank, project: 11261/ 1759), the BMBF (Bundesministerium für Bildung und Forschung: NBL 3), and the MeDDrive program of the Faculty of Medicine Carl Gustav Carus of the Dresden University of Technology.

References

1. M. Szkulmowski, A. Szkulmowska, T. Bajraszewski, A. Kowalczyk, and M. Wojtkowski, "Flow velocity estimation using joint spectral and time domain optical coherence tomography," *Opt. Express* **16**, 6008–6025 (2008).
2. A. Szkulmowska, M. Szkulmowski, A. Kowalczyk, and M. Wojtkowski, "Phase-resolved Doppler optical coherence tomography—limitations and improvements," *Opt. Lett.* **33**, 1425–1427 (2008).
3. M. Meinke, G. Müller, J. Helfmann, and M. Friebel, "Optical properties of platelets and blood plasma and their influence on the optical behavior of whole blood in the near infrared wavelength range," *J. Biomed. Opt.* **12**, 014024 (2007).
4. G. B. Jeffrey, "The motion of ellipsoidal particles immersed in a viscous fluid," *Proc. R. Soc. A* **102**, 161–179 (1922).
5. H. Schmid-Schönbein and R. Wells, "Fluid drop-like transition of erythrocytes under shear," *Science* **18**, 288–291 (1969).
6. M. Bitbol, "Red blood cell orientation in orbit $C = 0$," *Biophys. J.* **49**(5), 1055–1068 (1986).
7. M. Friebel, J. Helfmann, G. Müller, and M. Meinke, "Influence of shear rate on the optical properties of human blood in the spectral range 250 to 1100 nm," *J. Biomed. Opt.* **12**, 054005 (2007).
8. V. S. Lee and L. Tarassenko, "Absorption and multiple scattering by suspensions of aligned red blood cells," *J. Opt. Soc. Am. A* **8**, 1135–1141 (1991).
9. L.-G. Lindberg and P. A. Öberg, "Optical properties of blood in motion," *Opt. Eng.* **32**, 253–257 (1993).
10. A. Roggan, M. Friebel, K. Dörschel, A. Hahn, and G. Müller, "Optical properties of circulating human blood in the wavelength range 400–2500 nm," *J. Biomed. Opt.* **4**, 36–46 (1999).
11. R. Bayer, S. Çağlayan, and B. Günther, "Discrimination between orientation and elongation of RBC in laminar flow by means of laser diffraction," *Proc. SPIE* **2136**, 105–113 (1994).
12. J. Walther, A. Krüger, M. Cuevas, and E. Koch, "Effects of axial, transverse, and oblique sample motion in FD OCT in systems with global or rolling shutter line detector," *J. Opt. Soc. Am. A* **25**, 2791–2802 (2008).
13. J. Walther, G. Mueller, H. Morawietz, and E. Koch, "Signal power decrease due to fringe washout as an extension of the limited Doppler flow measurement range in spectral domain optical coherence tomography," *J. Biomed. Opt.* **15**, 041511 (2010).
14. D. J. Faber, E. G. Mik, M. C. G. Aalders, and T. G. van Leeuwen, "Toward assessment of blood oxygen saturation by spectroscopic optical coherence tomography," *Opt. Lett.* **30**, 1015–1017 (2005).
15. C.-W. Lu, C.-K. Lee, M.-T. Tsai, Y.-M. Wang, and C. C. Yang, "Measurement of the hemoglobin oxygen saturation level with spectroscopic spectral-domain optical coherence tomography," *Opt. Lett.* **33**, 416–418 (2008).
16. J. Moger, S. J. Matcher, C. P. Winlove, and A. Shore, "Measuring red blood cell flow dynamics in a glass capillary using Doppler optical coherence tomography and Doppler amplitude optical coherence tomography," *J. Biomed. Opt.* **9**, 982–994 (2004).
17. V. J. Srinivasan, J. Y. Jiang, M. A. Yaseen, H. Radhakrishnan, W. Wu, S. Barry, A. E. Cable, and D. A. Boas, "Rapid volumetric angiography of cortical microvasculature with optical coherence tomography," *Opt. Lett.* **35**, 43–45 (2010).
18. S. Meissner, G. Mueller, J. Walther, H. Morawietz, and E. Koch, "In-vivo Fourier domain optical coherence tomography as new tool for investigation of vasodynamics in the mouse model," *J. Biomed. Opt.* **14**, 034027 (2009).

19. A. I. Kholodnykh, I. Y. Petrova, K. V. Larin, M. Motamedi, and R. O. Esenaliev, "Precision of measurement of tissue optical properties with optical coherence tomography," *Appl. Opt.* **42**, 3027–3037 (2003).
20. P. Cimalla, J. Walther, M. Mehner, M. Cuevas, and E. Koch, "Simultaneous dual-band optical coherence tomography in the spectral domain for high resolution in vivo imaging," *Opt. Express* **17**, 19486–19500 (2009).
21. J. Walther, G. Mueller, H. Morawietz, and E. Koch, "Analysis of *in vitro* and *in vivo* bidirectional flow velocities by phase-resolved Doppler Fourier-domain OCT," *Sens. Actuators A: Phys.* **156**, 14–21 (2009).
22. J. Walther and E. Koch, "Transverse motion as a source of noise and reduced correlation of the Doppler phase shift in spectral domain OCT," *Opt. Express* **17**, 19698–19713 (2009).
23. T. R. Gregory, Animal Genome Size Database, <http://www.genomesize.com/cellsizes/>, (2001), 08/22/2011.
24. J. Walther, G. Mueller, S. Meissner, P. Cimalla, H. Homann, H. Morawietz, and E. Koch, "Time-resolved blood flow measurement in the *in vivo* mouse model by optical frequency domain imaging," *Proc. SPIE* **7372**, 73720J (2009).
25. S. H. Yun, G. Tearney, J. de Boer, and B. Bouma, "Motion artifacts in optical coherence tomography with frequency-domain ranging," *Opt. Express* **12**, 2977–2998 (2004).